J. Phys.: Condens. Matter **11** (1999) 7095–7102. Printed in the UK PII: S0953-8984(99)05763-X

Real-time kinetic neutron powder diffraction study of the phase transition from α-Mn to β-Mn

J R Stewart† and R Cywinski

School of Physics and Astronomy, University of St Andrews, North Haugh, St Andrews, Fife KY16 9SS, UK

Received 6 July 1999, in final form 10 August 1999

Abstract. High-resolution kinetic neutron powder diffraction has been used to study the kinetic properties of the α-Mn–β-Mn phase transition. This study reveals that the α-Mn–β-Mn phase transition is homogeneous. The rearrangement of the Mn atomic positions in the α- and β-phases is discussed in terms of their influence on the low-temperature magnetic properties of elemental Mn.

1. Introduction

Mn exists in four allotropic modifications at ambient pressure. The body-centred cubic (bcc) α-Mn phase is stable at ambient pressure to a temperature of 1000 K. α-Mn forms with space group $I\bar{4}3m$ with 58 atoms per unit cell and four non-equivalent crystallographic sites at Wyckoff positions 2a, 8c, and two sets at 24g [1]. The α-Mn structure is depicted in figure 1(a). Between 1000 K and 1370 K, the simple cubic β-Mn phase forms with space group $P4_132$ containing 20 atoms shared between two inequivalent crystallographic sites at Wyckoff positions 8c and 12d [3, 4] (see figure 1(b)). For the next 40 K between 1370 K and 1410 K, face-centred cubic (fcc) γ-Mn is formed, and from 1410 K up to the melting point of Mn at 1517 K, we find bcc δ-Mn.

The β-phase of elemental Mn can be readily retained at room temperature by rapid quenching of pure Mn ingots into water. γ-Mn undergoes a martensitic transition to a metastable face-centred tetragonal (fct) structure along with a concomitant antiferromagnetic phase transition on quenching to room temperature. Attempts to obtain metastable δ-Mn by quenching various Mn alloys have proved unsuccessful [5]. The pressure–temperature phase diagram of elemental Mn [2] is shown in figure 2.

β-Mn does not order magnetically down to the lowest temperatures, unlike both α-Mn and metastable fct γ-Mn, which show antiferromagnetic order at $T_N = 95$ K and 511 K respectively. The formation of long-range magnetic order in pure Mn and alloys such as the C15 cubic Laves phase YMn_2 is intimately linked to the Mn–Mn near-neighbour separation in these metals, with itinerant magnetic moments forming on relatively well-localized Mn atoms. It is, therefore, surprising that α-Mn supports long-range antiferromagnetic order and that β-Mn does not, since the mean volume per Mn atom is 12.11 Å^3 in α-Mn increasing to 12.60 Å^3 in β-Mn. It has further been suggested that topological frustration of the site II Mn atoms prohibits moment localization and magnetic order in β-Mn. Figure 1(b) depicts the

† Author to whom any correspondence should be addressed. Present address: Institut Laue–Langevin, 6, rue Jules Horowitz, BP 156, 38042 Grenoble, France.

0953-8984/99/377095+08$30.00

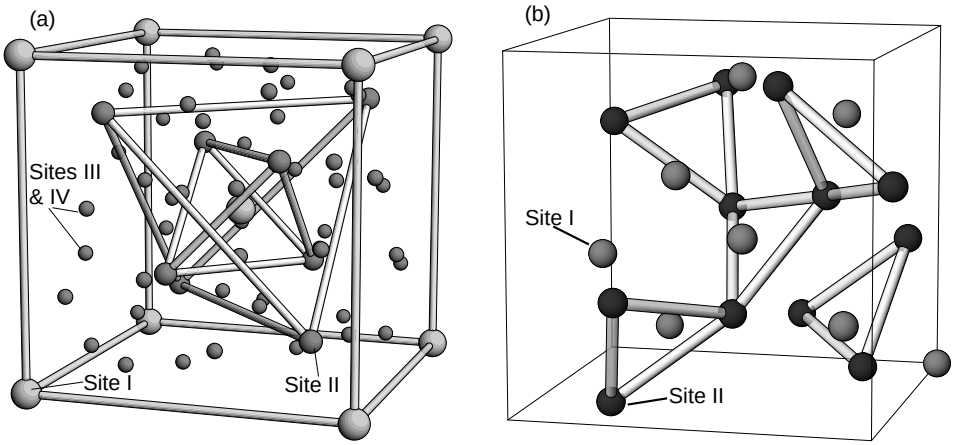

Figure 1. The (a) α-Mn and (b) β-Mn crystal structures.

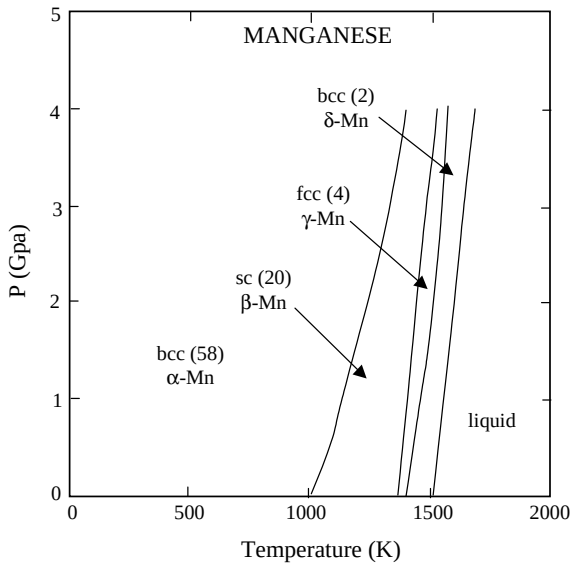

Figure 2. The phase diagram of manganese [2].

triangularly coordinated site II Mn atoms in the so-called 'distorted windmill' arrangement highlighted by Nakamura and co-workers [6]. This arrangement is, essentially, a quasi-two-dimensional lattice of corner-sharing triangles.

As part of a wider investigation of the structural and magnetic properties of β-Mn [8] we have studied the α-Mn–β-Mn phase transition using high-resolution kinetic neutron powder diffraction. This study was undertaken in order to characterize the nature of the phase transformation and to gain insight into the structural properties inherent in α-Mn and β-Mn, which support the formation of an antiferromagnetic ground state in α-Mn and prevent long-range magnetic order in β-Mn.

2. Isothermal phase transformations

In a homogeneous transformation, all regions of the system have an equal probability of transforming in a given time which is proportional to the untransformed volume remaining at that time. A transformation from state α to state β can thus be expressed in terms of the differential rate equation

$$\frac{\mathrm{d}V_\beta}{\mathrm{d}t} = k(V - V_\beta) \tag{1}$$

where V_β is the volume of the transformed region, V is the total volume of the system and k is the rate constant. Defining the β-phase fraction $S_\beta = V_\beta/V$, equation (1) can be solved to obtain

$$S_\beta = 1 - \exp(-t/\tau) \tag{2}$$

where $\tau = 1/k$ is the time constant of the phase transformation.

In nucleation and growth transformations it is assumed that a nucleation centre is formed at a time t_0 called the induction period. It is found experimentally that any dimension of the transformed region increases linearly with time, until the transformed regions impinge on each other, thereby interfering with each other's growth rates. This problem is essentially geometrical and was first addressed by Johnson and Mehl [9], and later by Avrami [10–12]. Avrami proposed that nucleation and growth transformations may be described in terms of the general equation

$$S_\beta = 1 - \exp[(-t/\tau)^n] \tag{3}$$

where the exponent n represents the dimensionality of the growth of the nucleated regions as shown in table 1. Equation (3) is known as the Avrami–Johnson–Mehl (AJM) equation. If the exponent $n = 1$, the AJM equation reduces to (2) and the transformation is homogeneous.

Table 1. Type of growth process indicated by the exponent n in the AJM equation.

Exponent n	Type of growth
1	Homogeneous
$1 \leqslant n < 2$	One dimensional—*dendritic*
$2 \leqslant n < 3$	Two dimensional—*plate-like*
$3 \leqslant n < 4$	Three dimensional

3. Experimental procedure

The powder diffraction spectra in this study were obtained using the High Resolution Powder Diffractometer, HRPD, at the ISIS pulsed neutron source, UK. The finely powdered Mn samples were placed in a vanadium sample can of 12 mm diameter and inserted into a standard ISIS furnace, able to cover a temperature range of 300 K to 1200 K. The Mn samples were held at a temperature of 500 °C for at least one hour before the temperature was raised rapidly at $t = 0$ to the temperature at which the isothermal transformation curve was to be measured. This ensured that the sample was phase-pure α-Mn at $t = 0$. Raising the temperature from 500 °C to slightly above the phase transition temperature of ∼700 °C took approximately 5 min. The excellent temperature control of the sample furnace on HRPD ensured a minimal overshoot of the desired temperature. Diffraction patterns were collected kinetically over time slices of between 5 and 15 min depending on the rate of the phase transformation. A five-minute measurement was found to be the shortest practical time slice on HRPD.

4. Results

Figure 3 shows a typical measurement of the α–β-Mn phase transition. The observed diffraction patterns are shown as a function of time at a constant temperature of 710 °C. Four such measurements were performed at temperatures of 700 °C, 705 °C, 710 °C and 715 °C. The β-Mn phase fraction S_β at each time interval was obtained by full two-phase Reitveld refinement of the measured diffraction patterns using the 'General Structure Analysis System' (GSAS) suite of programs [13]. A typical GSAS refinement is shown in figure 4. The time dependence of S_β at each temperature is shown in figure 5. The solid lines shown in figure 5 are fits to the data of the AJM equation (3). The time constants and exponents found in the fits are presented in table 2.

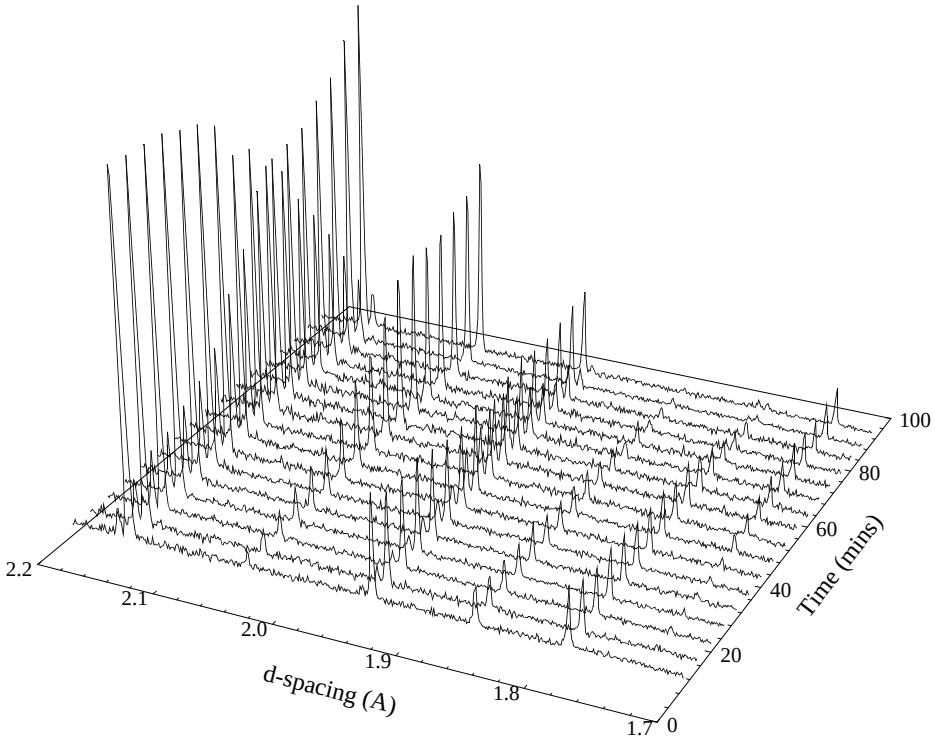

Figure 3. α-Mn to β-Mn phase transition at a temperature of 710 °C. The spectra shown represent ten-minute time slices.

Table 2. The time constant τ and exponent n for the α–β-Mn phase transition at the temperatures shown, found by fitting the data in figure 5 to the AJM equation (3).

Temperature (°C)	τ (min)	n
700 ± 0.5	310 ± 10	0.79 ± 0.03
705 ± 0.5	175 ± 2	1.05 ± 0.01
710 ± 0.5	34.0 ± 0.3	1.04 ± 0.02
715 ± 0.5	9.7 ± 0.2	1.17 ± 0.06

The form of the AJM equation implies that the α–β-Mn transformation curves should

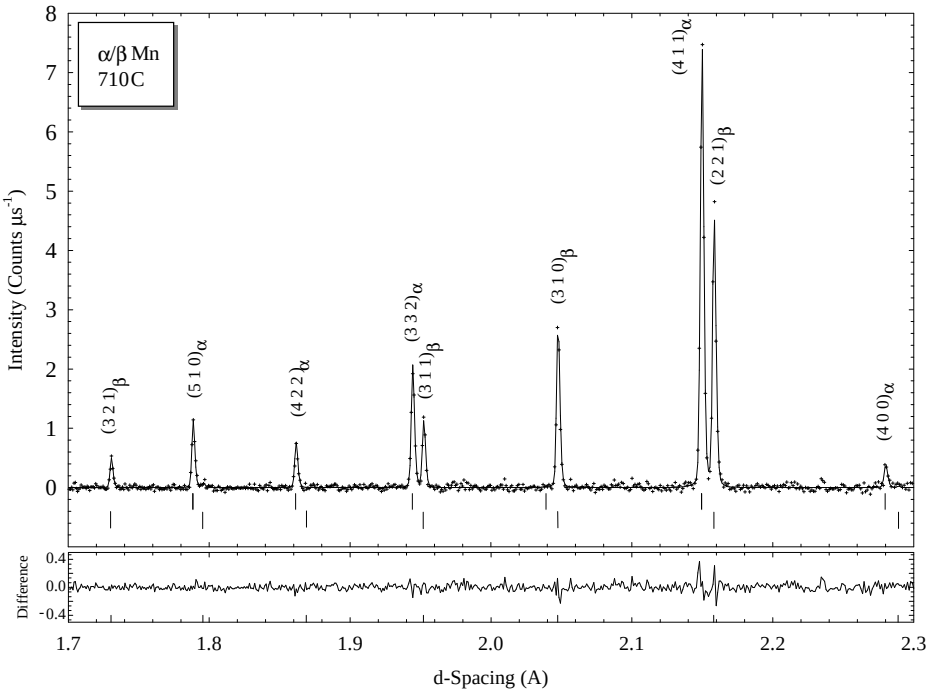

Figure 4. Typical two-phase Reitveld refinement of an α/β-Mn powder diffraction spectrum measured at 710 °C, and started 50 min into the measurement. The diffraction pattern was collected in 10 min. The α-Mn and β-Mn reflections are indicated by the subscripts shown in the figure.

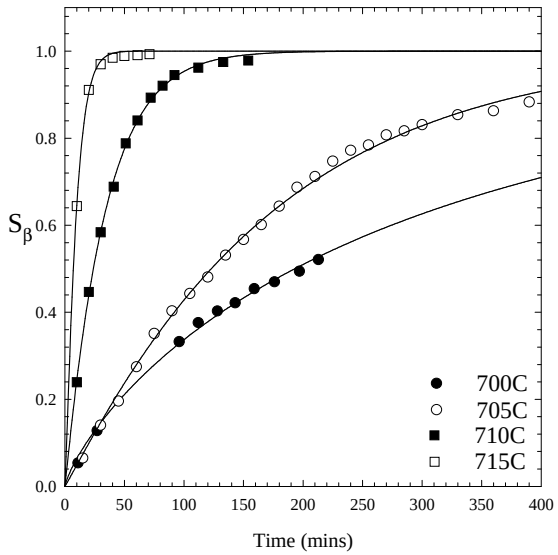

Figure 5. Measured time and temperature dependence of the β-Mn phase fraction S_β for the α–β-Mn transition. The lines shown are fits to the AJM equation (3).

scale with respect to time. This is demonstrated in figure 6 which shows the four isothermal transformation curves plotted in straight-line form:

$$\ln\ln\left(\frac{1}{1-S_\beta}\right) = n\ln\left(\frac{t}{\tau}\right) \tag{4}$$

as a function of t/τ. The isothermal transformation curves scale well with an average gradient of $n = 1.04 \pm 0.02$.

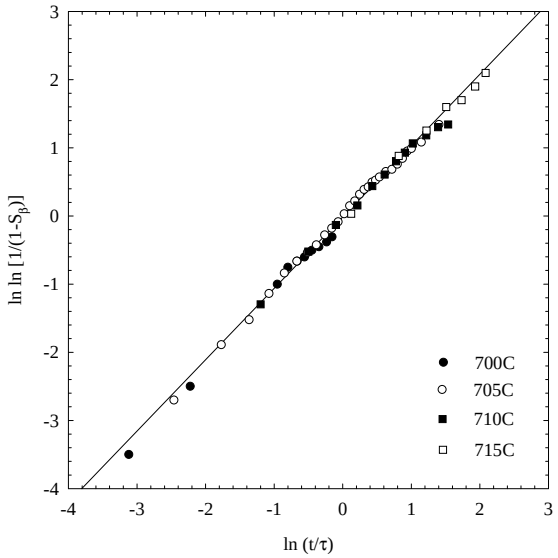

Figure 6. Graph of $\ln\ln(1/1 - S_\beta)$ against $\ln(t/\tau)$ demonstrating the scaling behaviour of the β-Mn phase fraction expressed in the form of a straight line of slope n. n is found to be 1.04 ± 0.02 for the α–β-Mn phase transition.

5. Discussion

The value of the exponent $n = 1$ found in this study implies that the α–β-Mn phase transition is homogeneous throughout the sample. This is perhaps not surprising since the phase transformation is rather subtle, involving a very slight volume expansion with both phases displaying cubic symmetry as shown in figures 3 and 4. We might therefore expect that the free-energy difference at the interface between the two phases is extremely small, leading to homogeneous nucleation of the β-Mn phase. The metastable β–α-Mn phase transformation which occurs at $\sim$230 °C has been shown by Husband and co-workers [14] to transform according to the AJM equation with an exponent of $n = 4$. This is due to the large drop in free energy from the local free-energy minimum associated with the metastable β-Mn phase to the α-Mn free energy, leading to a large free-energy barrier at the interface between the transformed regions and nucleation centres. Similar behaviour has been observed in the α–β-Sn and β–α-Sn transformations which have exponents of $n = 2$ and $n = 5$ respectively [15]. As can be seen from figure 4, the major peaks of α-Mn and β-Mn are very close in d-spacing. The general relationship between the unit cells is such that

$$(h_\alpha^2 + k_\alpha^2 + l_\alpha^2) = 2(h_\beta^2 + k_\beta^2 + l_\beta^2). \tag{5}$$

Thus, the (4 1 1)/(3 3 0) peak for α-Mn transforms to the (3 0 0)/(2 2 1) peak for β-Mn. Likewise, the (3 3 2) peak for α-Mn transforms to the (3 1 1) peak for β-Mn. This implies that the room temperature lattice constants of α- and β-Mn (8.89 Å and 6.32 Å respectively) are such that

$$a_\alpha \simeq \sqrt{2}\, a_\beta .$$

The change of symmetry is accompanied by an overall lattice expansion of $\Delta d/d = 4 \times 10^{-3}$.

6. Conclusions

We have investigated the transformation kinetics of the α-Mn–β-Mn phase transformation using high-resolution neutron powder diffraction. The form of the observed isothermal α–β-Mn transformation curves is well described by the Avrami–Johnson–Mehl (AJM) equation with an exponent $n = 1$, implying that the α–β-Mn phase transition is homogeneous. The phase transition involves a subtle change of symmetry with the $\langle 1\,0\,0 \rangle$ planes of the $I\bar{4}3m$ α-Mn phase forming the $\langle 1\,1\,0 \rangle$ planes of the $P4_132$ β-Mn phase, with an associated 0.4% linear expansion of the lattice. While a net expansion of the lattice might be expected to result in a greater distance between neighbouring Mn atoms, and hence favour the formation of local magnetic moments, as has been observed in our muon spin-relaxation (μSR) studies of β-MnAl [7], analysis of the Mn–Mn near-neighbour distances found in the current study and shown in table 3 reveals that the β-Mn structure exhibits more uniform atomic packing than α-Mn with neither of the near-neighbour distances associated with sites I and II in the β-Mn structure as large as that found for site I in the α-Mn structure. In the antiferromagnetic state at $T < 95$ K, α-Mn is thought to possess localized magnetic moments on site I, the site with the largest near-neighbour separation in the α-Mn matrix [16]. The shorter near-neighbour distances in the β-Mn structure may therefore prevent moment localization in the matrix. In addition, it is likely that frustration between the triangularly coordinated site II Mn atoms in the β-Mn structure will prevent long-range magnetic order [6].

Table 3. α- and β-Mn near-neighbour distances at 700 °C for each of the crystallographic sites shown (defined in section 1).

Site	α-Mn NN distance (Å)	β-Mn NN distance (Å)
I	2.81	2.41
II	2.62	2.70
III	2.41	
IV	2.41	

Acknowledgments

The authors are indebted to Dr R M Ibberson of the ISIS pulsed neutron facility for experimental support, and to the Engineering and Physical Sciences Research Council for financial support.

References

[1] Bradley A J and Thewlis J 1927 *Proc. R. Soc.* A **115** 456
[2] Young D A 1991 *Phase Diagrams of the Elements* (Berkeley, CA: University of California Press)
[3] Kripyakevich P I 1960 *Sov. Phys.–Crystallogr.* **5** 253

[4] Nakai Y, Oyamatsu H and Kunitomi N 1989 *J. Phys. Soc. Japan* **58** 2805
[5] Basinski Z S and Christian J W 1949 *Proc. R. Soc.* A **223** 554
[6] Nakamura H, Yoshimoto K, Shiga M, Nishi M and Kakurai K 1997 *J. Phys.: Condens. Matter* **9** 4701
[7] Stewart J R and Cywinski R 1999 *Phys. Rev.* B **59** 4305
[8] Cywinski R, Kilcoyne S H and Stewart J R 1999 *Physica* B **267+268** 88
[9] Johnson W A and Mehl R F 1938 *Trans. Am. Inst. Mineral. (Metall.) Eng.* **135** 416
[10] Avrami M 1939 *J. Chem. Phys.* **7** 1103
[11] Avrami M 1940 *J. Chem. Phys.* **8** 212
[12] Avrami M 1941 *J. Chem. Phys.* **9** 177
[13] Larson A C and Von Dreele R B 1994 GSAS: general structure analysis system *Los Alamos National Laboratory Report* LAUR 86-748
[14] Husband J N 1959 unpublished
[15] Iizumi M 1986 *Physica* B **136** 36
[16] De Doncker P 1988 *J. Physique Coll.* **49** C8 81